Available online at www.sciencedirect.com
ScienceDirect
International Journal of Heat and Mass Transfer 51 (2008) 920–928
International Journal of HEAT and MASS TRANSFER
www.elsevier.com/locate/ijhmt

Unsteady heat transfer from an elliptic cylinder

Gheorghe Juncu *

POLITEHNICA University Bucharest, Catedra Inginerie Chimica, Polizu 1, 78126 Bucharest, Romania

Received 16 May 2007; received in revised form 11 September 2007

Abstract

Numerical methods are used to investigate the transient heat transfer from an elliptic cylinder to a steady stream of viscous, incompressible fluid. The temperature of the cylinder is considered spatially uniform but not constant in time. The momentum and heat balance equations were solved numerically in elliptic coordinate system. The solutions span the parameter ranges $5 \leqslant Re \leqslant 40$, $1 \leqslant Pr \leqslant 100$ and axis ratio ε, $0.1 \leqslant \varepsilon \leqslant 0.75$. The computations were focused on the influence of the axis ratio and volume heat capacity ratio on the heat transfer rate.

Keywords: Unsteady heat transfer; Forced convection; Elliptic cylinder; Laminar flow; Finite difference method

1. Introduction

In many industrial applications, where heat loads are substantial and space is limited, the elliptical geometry outperforms the circular geometry. Elliptical cylinders offer less flow resistance and higher heat transfer rates than circular cylinders. In spite of this fact, the heat transfer from an elliptical cylinder is the subject of relatively few theoretical/numerical studies.

The laminar mixed (natural and forced) convective heat transfer from a straight isothermal tube of elliptic cross-section placed in a uniform stream was investigated numerically in [1]. The free stream direction is horizontal and normal to the tube axis and the flow field is two-dimensional. The effects of the Reynolds number, $20 \leqslant Re \leqslant 500$, Grashof number, $0 \leqslant Gr \leqslant 1.25 \times 10^6$, Prandtl number, Pr, axis ratio and the angle of inclination (varying from 0° to 180°) on the heat transfer process were studied. In [2] the two-dimensional steady-state problem of laminar forced convective heat transfer from an isothermal cylinder, elliptic in cross section, inclined to a uniform stream is investigated. Numerical solutions of the Navier–Stokes and energy equations have been obtained for Reynolds numbers, Re, 5 and 20, Prandtl number, Pr, and inclination angle θ in the ranges, $1 \leqslant Pr \leqslant 25$ and $0 \leqslant \theta \leqslant \pi/2$. For large Pe values, the average rate of heat transfer, Nu, was found to behave closely to the theoretical result $Nu \approx Pe^{1/3}$, where $Pe = RePr$ is the Peclet number. D'Alessio discussed in [3] the two-dimensional problem of forced convection past an inclined elliptic cylinder. Both the steady state and unsteady state cases have been considered for moderate Reynolds numbers, $40 \leqslant Re \leqslant 70$ and Prandtl number $Pr = 1$. Badr [4] analysed numerically the laminar forced convection from a straight isothermal tube of elliptic cross-section placed in a uniform stream. For Reynolds number in the range 20–500, it is shown that: (a) the heat transfer reaches its maximum value when the angle of inclination is null while the minimum occurs when the angle of inclination is equal to $\pi/2$; (b) when the angle of inclination is equal to zero, smaller axis ratio gives higher heat transfer rates. Forced and mixed convective heat transfer from accelerated flow past an elliptic cylinder was investigated in [5]. The fluid is considered viscous and incompressible and the flow laminar and two-dimensional. The elliptic cylinder is inclined at an angle θ with the horizontal and starting from rest, accelerates uniformly through the fluid. The temperature of the cylinder

* Tel./fax: +40 21 345 0596.
E-mail addresses: juncu@easynet.ro, juncugh@netscape.net

0017-9310/$ - see front matter © 2007 Elsevier Ltd. All rights reserved.
doi:10.1016/j.ijheatmasstransfer.2007.11.001

Nomenclature

a	semi-major axis of elliptical cylinder
b	semi-minor axis of elliptical cylinder
c	focal distance
c_P	heat capacity
e	dimensionless focal distance or eccentricity, c/a
Pr	Prandtl number, $Pr = \mu/\alpha$
Re	Reynolds number, $Re = 2U_\infty a/\mu$
t	time
T	temperature
U_∞	free stream velocity
X	streamwise (horizontal) Cartesian coordinate
Y	transverse (vertical) Cartesian coordinate
Z	dimensionless temperature defined by the relations, $Z_{(c)} = \frac{T_{f(c)} - T_{f,\infty}}{T_{c,0} - T_{f,\infty}}$

Greek symbols

α	thermal diffusivity of the fluid phase
ε	axis ratio, b/a
μ	kinematic viscosity
ρ	density
τ	dimensionless time or Fourier number, $\tau = t\alpha/a^2$
ω	dimensionless vorticity
ψ	dimensionless stream function
Ξ	volume heat capacity ratio, $(\rho_c\ c_{P,c})/(\rho_f c_{P,f})$

Subscripts

c	refers to cylinder
f	refers to the fluid
0	initial conditions
∞	large distance from the cylinder

surface is constant. Khan et al. [6] used the Von Karman–Pohlhausen integral method to solve the boundary layer momentum and energy equations. Isothermal and isoflux thermal boundary conditions were considered on the surface of the cylinder. Three general correlations, one for drag and two for heat transfer, have been determined. The drag and the average heat transfer coefficients depend on the Reynolds number as well as on the axis ratio. It must be also mentioned that in [5] the experimental studies dedicated to fluid flow around and heat transfer from elliptical cylinders are reviewed.

In the articles mentioned previously the temperature of the cylinder is considered constant. A constant temperature inside the cylinder indicates the presence of a heat source in the system. When there is no heat source in the system, the heat transfer problem should be rewritten and solved as an unsteady conjugate heat transfer problem. The internal and external problems are the asymptotic formulations of the conjugate problem. The usefulness and at the same time the necessity of a study dedicated to the internal and external problems can be twofold argued. First, there are enough real life situations well described by these models. Secondly, when solving the conjugate problem, the asymptotic solutions play an important role.

The aim of this paper is to extend the previous studies to the case of elliptic cylinders with spatially uniform, but changing with time, temperature (i.e. to solve the external problem). The influence of the volume heat capacity ratio and axis ratio on the heat transfer rate is investigated for $Re = 5$, 10.0, 25.0, 40.0 (Re is the cylinder Reynolds number based on the major axis) and three values of the Prandtl number, $Pr = 1$, 10 and 100. From our knowledge, this problem was not investigated until now.

2. Model equations

Consider uniform flow of a Newtonian fluid past a fixed elliptic cylinder with major axis $2a$ and minor axis $2b$. The cylinder is oriented so that the major axis is parallel to the free stream flow direction. The flow is assumed to be laminar, steady and two-dimensional. The free stream velocity and temperature are denoted by U_∞ and $T_{f,\infty}$, respectively. The following statements are considered valid:

- the effects of buoyancy and viscous dissipation are negligible;
- the physical properties of the material of the cylinder and the fluid are considered to be uniform, isotropic and constant;
- no emission or absorption of radiant energy;
- no phase change.

The condition of spatially uniform temperature inside the cylinder is fulfilled if the relaxation time inside the cylinder is considerably smaller than the relaxation time in the fluid. The transfer is hundreds of times (at least) faster inside the cylinder than in the fluid. In terms of physical quantities, this condition means values considerably greater than one for the conductivity ratio (the conductivity ratio is defined as (cylinder's thermal conductivity)/(fluid thermal conductivity)).

The Cartesian coordinate system is not convenient for either analytical or numerical purposes. The conformal transformation

$$X + iY = \cosh(\xi + i\eta)$$

generates a coordinate system (elliptic cylindrical coordinates, [7]) that is better suited to the geometry of the prob-

lem. The relation between the elliptic coordinates (ξ,η) and the Cartesian coordinates (X, Y) is:

$$X = c\cosh\xi\cos\eta, \quad Y = c\sinh\xi\sin\eta$$

where c is the focal distance

$$c = a\sqrt{1-\varepsilon^2}, \quad \varepsilon = \frac{b}{a}.$$

The surface of the ellipse is defined by $\xi = \xi_0$, so that $\tanh\xi_0 = \varepsilon$. This transformation maps the upper half of the XY–plane (which by symmetry is all that need to be considered) into the semi-infinite strip $\xi \geqslant \xi_0$, $0 \leqslant \eta \leqslant \pi$.

Nondimensionalizing the basic conservation balances for momentum and thermal energy using the free stream fluid properties and the semi-major axis, we obtain the governing differential equations:

– fluid motion

$$\frac{\partial^2\psi}{\partial\xi^2} + \frac{\partial^2\psi}{\partial\eta^2} = -J\omega \tag{1a}$$

$$\frac{Re}{2}\left(\frac{\partial\psi}{\partial\eta}\frac{\partial\omega}{\partial\xi} - \frac{\partial\psi}{\partial\xi}\frac{\partial\omega}{\partial\eta}\right) = \frac{\partial^2\omega}{\partial\xi^2} + \frac{\partial^2\omega}{\partial\eta^2} \tag{1b}$$

– energy

$$\frac{\partial Z}{\partial\tau} + \frac{RePr}{2J}\left(\frac{\partial\psi}{\partial\eta}\frac{\partial Z}{\partial\xi} - \frac{\partial\psi}{\partial\xi}\frac{\partial Z}{\partial\eta}\right) = \frac{1}{J}\left(\frac{\partial^2 Z}{\partial\xi^2} + \frac{\partial^2 Z}{\partial\eta^2}\right) \tag{2a}$$

$$\frac{\partial Z_c}{\partial\tau} = \frac{2}{\pi\varepsilon\Xi}\int_0^\pi \left.\frac{\partial Z}{\partial\xi}\right|_{\xi=0} \mathrm{d}\eta \tag{2b}$$

where $J = e^2(\sinh^2\xi + \sin^2\eta)$ and e is the dimensionless focal distance (or ellipse eccentricity).

The boundary conditions to be satisfied are;

– interface ($\xi = \xi_0$)

$$\psi = 0, \quad Z_c = Z \tag{3a}$$

– free stream ($\xi = \infty$)

$$\psi \to e\sinh\xi\cos\eta, \quad \omega \to 0,\ Z \to 0.0 \tag{3b}$$

– symmetry axis ($\eta = 0, \pi$)

$$\psi = \omega = 0, \quad \frac{\partial Z}{\partial\eta} = 0.0 \tag{3c}$$

The dimensionless initial conditions are:

$$\tau = 0.0, \quad Z_c = 1.0,\ Z(\xi > \xi_0) = 0.0 \tag{4}$$

The physical quantities of interest are the cylinder temperature Z_c, the instantaneous local Nusselt number, Nu_η, and the instantaneous average Nusselt number, Nu_{ext}. Considering as driving force the difference between the instantaneous cylinder temperature and the free stream temperature, the instantaneous local and average Nu numbers are given by

$$Nu_\eta = -\frac{2}{Z_c e\sqrt{\sinh^2\xi_0 + \sin^2\eta}}\left.\frac{\partial Z}{\partial\xi}\right|_{\xi=\xi_0} \tag{5a}$$

$$Nu_{ext} = -\frac{1}{E(e)Z_c}\int_0^\pi \left.\frac{\partial Z}{\partial\xi}\right|_{\xi=\xi_0} \mathrm{d}\eta \tag{5b}$$

where $E(e)$ is the complete elliptic integral of the second kind. The characteristic length used to define the Nu numbers is the major axis of the ellipse, $2a$.

3. Method of solution

The energy balance equations and the Navier–Stokes equations were solved numerically. The finite difference method was used for discretization.

The Navier–Stokes equations being uncoupled from the energy balance equations can be solved independently of them. The algorithm employed is the nested defect-correction iteration, [8,9]. Eq. (1a) was discretized with the central second order accurate finite difference scheme. A double discretization (upwind and central finite difference schemes), necessary for the defect correction iteration, was used for Eq. (1b). Numerical experiments were made with the discretization steps $\Delta\xi = \Delta\eta = \pi/64, \pi/128, \pi/256$.

Table 1
Drag coefficient values for $\varepsilon = 0.2$

Re	ξ_∞	Grid $N^1 \times M^2$	C_D	
			(3b)	(6)
5	3.344	65 × 65	2.9668	2.6421
		129 × 129	2.9659	2.6427
		257 × 257	2.9657	2.6429
	4.1297	65 × 81	2.7857	2.6460
		129 × 161	2.7849	2.6473
		257 × 321	2.7846	2.6476
	4.915	65 × 97	2.7102	2.6491
		129 × 193	2.7092	2.6508
		257 × 385	2.7090	2.6512
50	3.344	65 × 65	0.7082	0.6787
		129 × 129	0.7083	0.6793
		257 × 257	0.7085	0.6796
	4.1297	65 × 81	0.6923	0.6809
		129 × 161	0.6924	0.6816
		257 × 321	0.6925	0.6819
	4.915	65 × 97	0.6866	0.6816
		129 × 193	0.6866	0.6823
		257 × 385	0.6868	0.6826

1 – number of grid points in η-direction; 2 – number of grid points in ξ-direction.

Table 2
Comparison of the present C_D values with published results for $\varepsilon = 0.2$

Re	C_D	
	Present results	Sivakumar et al. [12][a]
25	1.0060	1.0143
200	0.3262	0.3281

[a] Transformed to the present characteristic length.

Table 3
Asymptotic Nu_{ext} values for $Re = 10$

ε	Pr	Ξ									$Z_c = 1.0$
		0.01	0.1	0.2	0.5	1.0	2.0	5.0	10.0	100.0	
Plate	1	0.016[a]	0.15[a]	0.29[a]	0.65	1.09	1.606	2.12	2.35	2.60	2.66
	10	0.11	0.97	1.694	3.05	4.01	4.70	5.22	5.40	5.583	5.62
	100	0.546	4.077	6.305	8.974	10.33	11.21	11.76	11.897	12.03	12.04
0.20	1	0.005[a]	0.05[a]	0.098[a]	0.238[a]	0.45[a]	0.809[a]	1.469	1.934	2.56	2.65
	10	0.039	0.368	0.704	1.536	2.48	3.51	4.575	5.05	5.548	5.61
	100	0.204	1.82	3.26	5.969	8.175	9.79	11.03	11.49	11.98	11.99
0.40	1	0.008[a]	0.077[a]	0.15[a]	0.355[a]	0.65[a]	1.10	1.74	2.09	2.483	2.53
	10	0.06[a]	0.56	1.04	2.10	3.09	3.97	4.715	5.01	5.298	5.33
	100	0.33	2.72	4.50	7.22	9.09	10.12	10.83	11.08	11.31	11.33
0.750	1	0.009[a]	0.084[a]	0.16[a]	0.387[a]	0.705[a]	1.149	1.695	1.952	2.22	2.25
	10	0.059[a]	0.55[a]	1.026[a]	2.07	2.978	3.71	4.266	4.47	4.67	4.69
	100	0.30[a]	2.597	4.31	6.75	8.12	8.94	9.48	9.67	9.85	9.86
1	1	0.0085[a]	0.075[a]	0.148[a]	0.35[a]	0.65[a]	1.065	1.567	1.795	2.029	2.06
	10	0.044[a]	0.419[a]	0.803[a]	1.723	2.61	3.329	3.861	4.06	4.237	4.26
	100	0.164[a]	1.56[a]	2.90[a]	5.457	7.014	7.913	8.488	8.68	8.855	8.87

[a] Unfrozen asymptotic value.

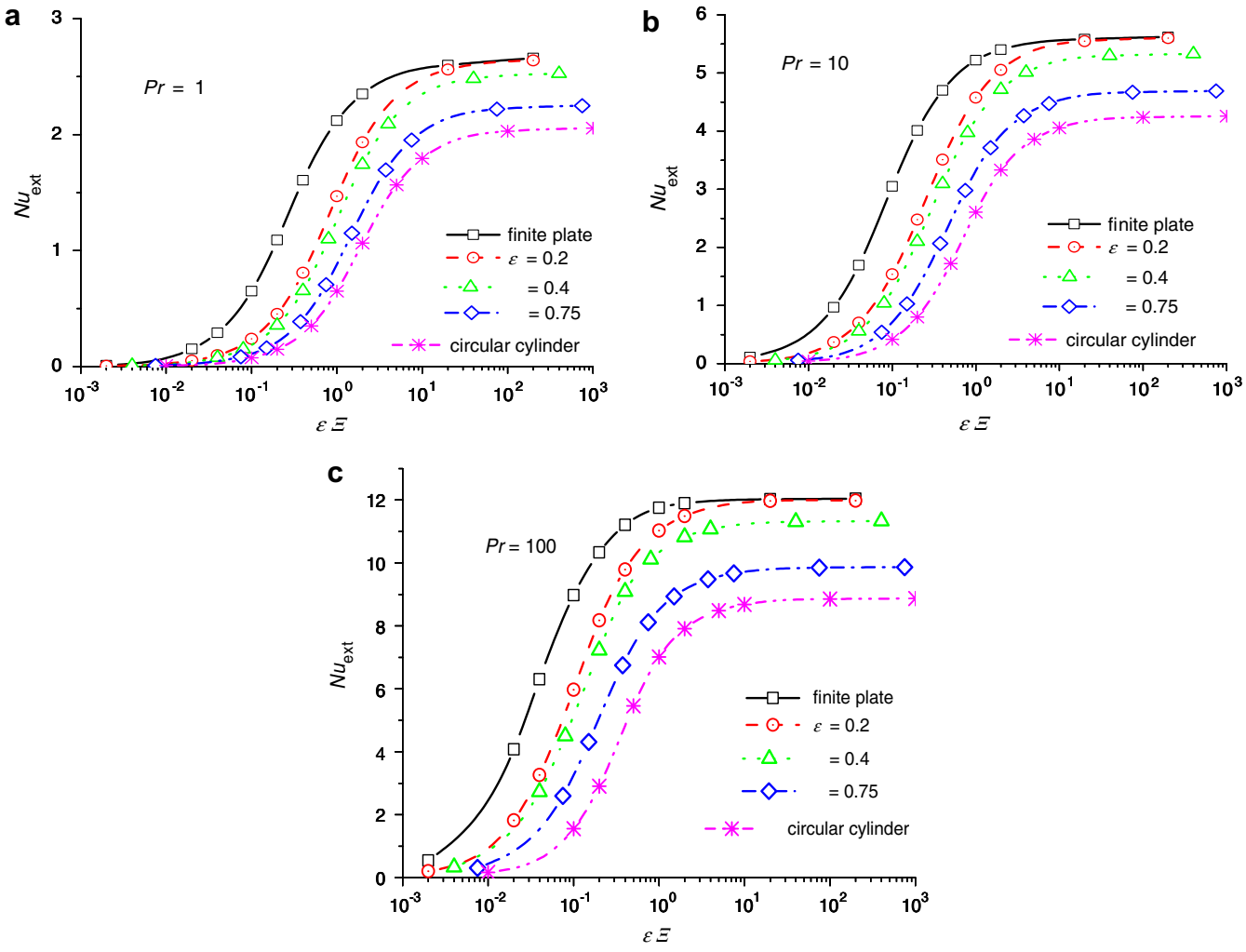

Fig. 1. Asymptotic values of the Nu numbers function of $\varepsilon\Xi$ for $Re = 10$; (a) $Pr = 1$; (b) $Pr = 10.0$; (c) $Pr = 100.0$.

The main problem in solving numerically the present Navier–Stokes equations is the boundary conditions at infinity. A reference study in this field may be considered [10]. According to [10], at ξ_∞, the boundary conditions

$$\frac{\partial\hat{\psi}}{\partial\xi}=\frac{\partial\omega}{\partial\xi}=0.0 \tag{6}$$

provide accurate results at moderate Re values. In (6), $\hat{\psi}=\psi-e\sinh\xi\sin\eta$ is the deviation from the uniform flow. In this work, both relations (3b) and (6) were used as boundary conditions at infinity.

The mathematical model equations (2a) and (2b) is a system formed by a 2D parabolic partial differential equation (PDE) that describes the heat transfer in the fluid phase and an ordinary differential equation (ODE) that describes the energy balance of the cylinder. Eq. (2a) was discretized with the exponentially fitted scheme, [11]. The discretization steps in both spatial directions are equal and took the values $\pi/64$, $\pi/128$ and $\pi/256$. Let us consider that the numerical values of the dimensionless temperature at time τ are known. The values at the time $\tau+\Delta\tau$ were calculated as follows: (i) the values on the cylinder's surface were calculated by integrating (2b) from τ to $\tau+\Delta\tau$ with an explicit modified Euler algorithm; the integral from relations (2b) was calculated by the Simpson 3/8 rule using the local heat flux values available at time τ; (ii) the values of the dimensionless temperature in the fluid phase were calculated by the implicit ADI method using the cylinder's surface values computed in the previous step as boundary conditions (relation (3a)).

The time step was variable and changed from the start of the computation to the final stage. The values of the time step depend on the parameter values.

4. Results

The heat transfer is characterized by the following dimensionless parameters: Re, Pr, ε and Ξ. The numerical simulations carried out in this work focused on axis ratio range 0.1–0.75. Four values of the Re number were selected: $Re=5.0$, 10.0, 25.0 and 40.0. We considered $Re=40.0$ as superior limit because we used the circular cylinder as boundary case. For the circular cylinder, it is well known that for $Re>Re_{crt}\cong 46$ the flow becomes

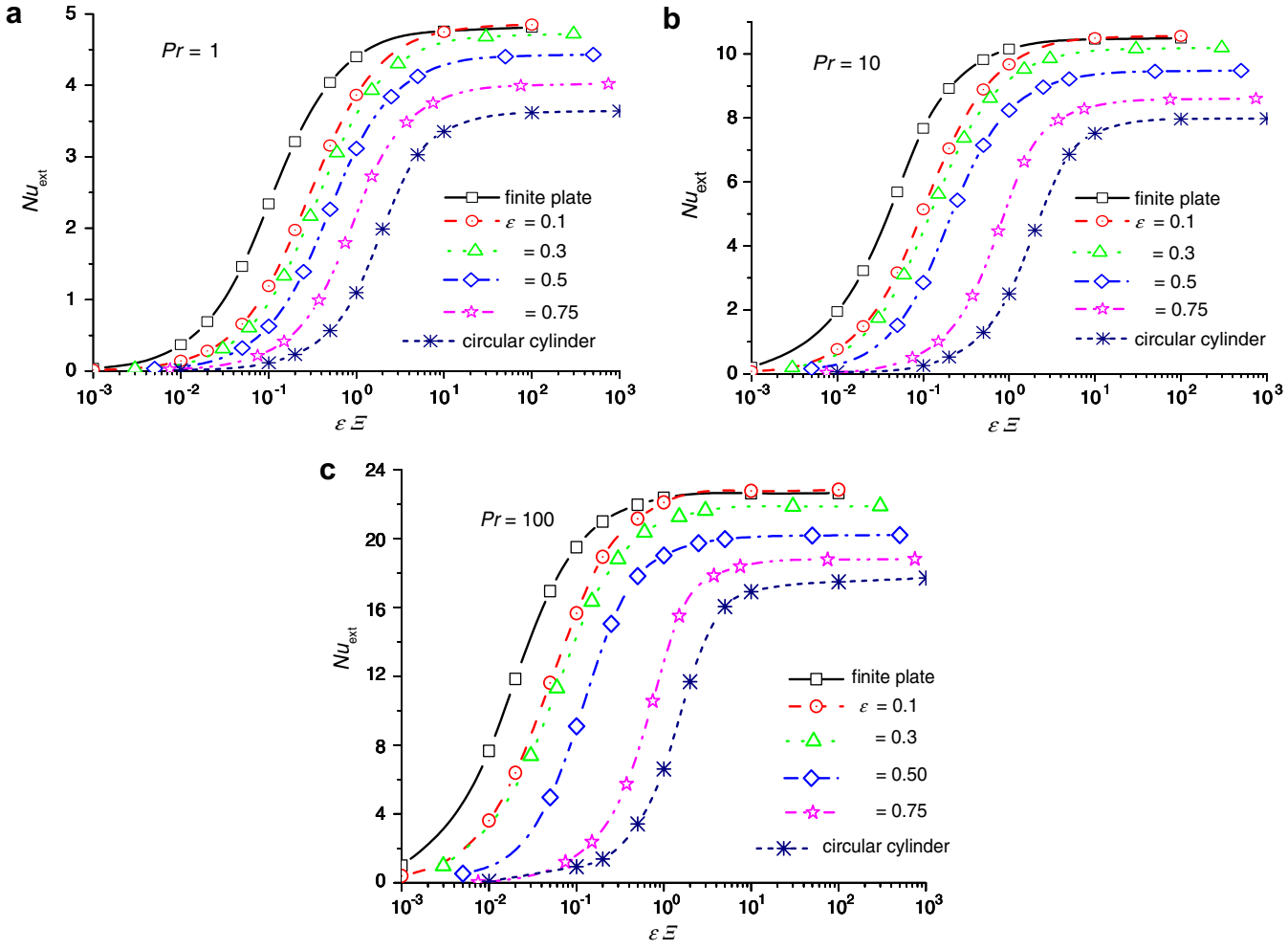

Fig. 2. Asymptotic values of the Nu numbers function of $\varepsilon\Xi$ for $Re=40$; (a) $Pr=1$; (b) $Pr=10.0$; (c) $Pr=100.0$.

unsteady. For each value of Re, Pr takes the following three values, $Pr = 1.0$, $Pr = 10.0$ and $Pr = 100.0$. Values of χ in the range 10^{-2}–10^{2} cover the situations of practical interest and allow the study of asymptotic behaviour.

The influence of the far field boundary conditions and grid step size on the drag coefficient C_D is shown in Table 1. Table 2 shows the comparison of the present results for the drag coefficient with the results published in [12]. In Tables 1 and 2 numerical experiments performed at Re values greater than those mentioned previously are presented.

For the elliptic cylinder the comparison of the drag coefficient values with previous published results it is not an elementary task because different authors used different characteristic lengths (for example, D'Alessio [3] and Badr [4] used the focal distance, D'Alessio and Dennis [2] the major axis, Sivakumar et al. [12] the minor axis and so on). We selected Sivakumar et al. [12] for the following reasons: (a) it is the most recent article; (b) the transformation from the characteristic length used in [12] to the present characteristic length is elementary; (c) the agreement between their results and other numerical solutions, [13–15], is very good.

Table 1 shows that the present numerical results obtained on a mesh with 257 × 385 points and the boundary condition (6) can be considered grid independent. Table 2 shows that the present numerical results are in good agreement with the results presented in [12]. The results presented in Tables 1 and 2 can be considered an argument for the accuracy of the present hydrodynamic computations.

Unfortunately, there are no data in literature to verify the accuracy of the present heat transfer computations. Based on the experience of the sphere, cylinder and finite plate problems, one may expect that, when χ tends to infinity, the asymptotic Nu values will tend to the Nu values corresponding to the elliptic cylinder with constant temperature. This aspect will be discussed in the next paragraphs of this section.

From the numerical experiments made we selected for presentation the asymptotic values of Nu_{ext} calculated for $Re = 10$ and 40 and the asymptotic values of Nu_η calculated for $Re = 20$, $Pr = 10$ and $\varepsilon\Xi = 0.1$, 1 and 10. This selection captures the salient features encountered during the numerical simulations. The asymptotic values of Nu_{ext} computed for $Re = 10$ are presented in Table 3 and plotted in Fig. 1. Fig. 2 shows the asymptotic Nu_{ext} values for $Re = 40$. The asymptotic values of the local Nu number for $Re = 20$ and $Pr = 10$ are presented in Fig. 3. In order to avoid a strong compression of the curves, in Fig. 3a and b the maximum value of the ordinate is smaller than the maximum values of the local Nu number for the

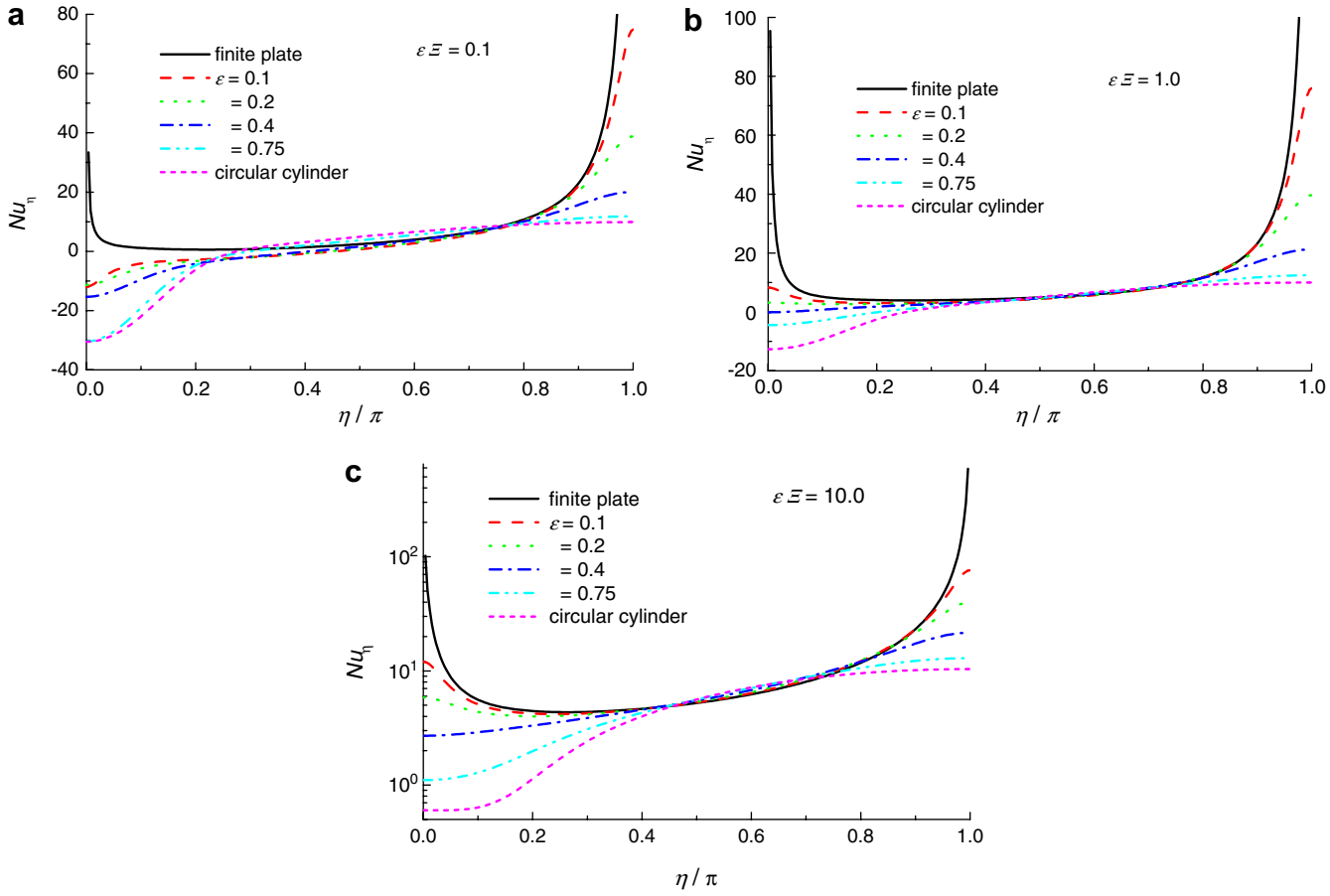

Fig. 3. Asymptotic values of the local Nu number for $Re = 20$ and $Pr = 10$; (a) $\varepsilon\Xi = 0.1$; (b) $\varepsilon\Xi = 1$; (c) $\varepsilon\Xi = 10$.

plate. In Fig. 3 the front stagnation point (leading edge) is $\eta = \pi$ while the rear stagnation point (trailing edge) is $\eta = 0$. The presence of the superscript * in a cell indicates that the time variation of the Nu number does not reach a frozen asymptotic value. The values depicted in this case correspond to the integration final, when the time variation of Nu_{ext} becomes small. The last column of Table 3 shows the values provided by the elliptic cylinder with constant temperature. The lines corresponding to plate depict the asymptotic Nu values calculated for the finite plate. The lines corresponding to $\varepsilon = 1$ show the asymptotic Nu values provided by the circular cylinder. In Figs. 1 and 2 the results obtained for $\Xi = 1000$ were taken into consideration. In all cases, the relative difference between Nu_{ext} ($\Xi = 1000$) and Nu_{ext} ($Z_c = 1$) was smaller than 1%.

In this work, the finite plate has length L and thickness h. Only one side of the plate, of length L, is wetted. The unwetted sides of the plate are insulated. In the mathematical model of the external problem of the finite plate [16], the volume heat capacity ratio and the aspect ratio h/L appear only as the product $(h/L)\Xi$ and may be considered a single parameter. Note that for the finite flat plate the aspect ratio does not influence the external flow. For the elliptic cylinder, the axis ratio appears explicitly in the mathematical model only in Eq. (2b), as the product $\varepsilon\Xi$, but the velocity profiles depend on ε. Thus, for a fair comparison between the flat plate, elliptic cylinder and circular cylinder, the following conventions were adopted: (a) the data presented in Table 3 and Figs. 1 and 2 for the flat plate were calculated considering $L = 2a$, h/L equal to 0.2 (Table 3 and Fig. 1) and 0.1 (Fig. 2); (b) in Figs. 1 and 2 the abscissa is $\varepsilon(h/L)\Xi$; Fig. 3 shows the asymptotic Nu_η values computed for the same $\varepsilon(h/L)\Xi$ value.

The results presented in Table 3 and Figs. 1–3 lead to the following observations:

- for given Re and Pr values, the axis ratio and the volume heat capacity ratio have a distinct influence on the asymptotic Nu values;
- for given Re, Pr and $\varepsilon\Xi$ values, the decrease in the axis ratio increases the asymptotic Nu_{ext} values; the finite plate and the circular cylinder may be considered the boundary cases for the elliptic cylinder;

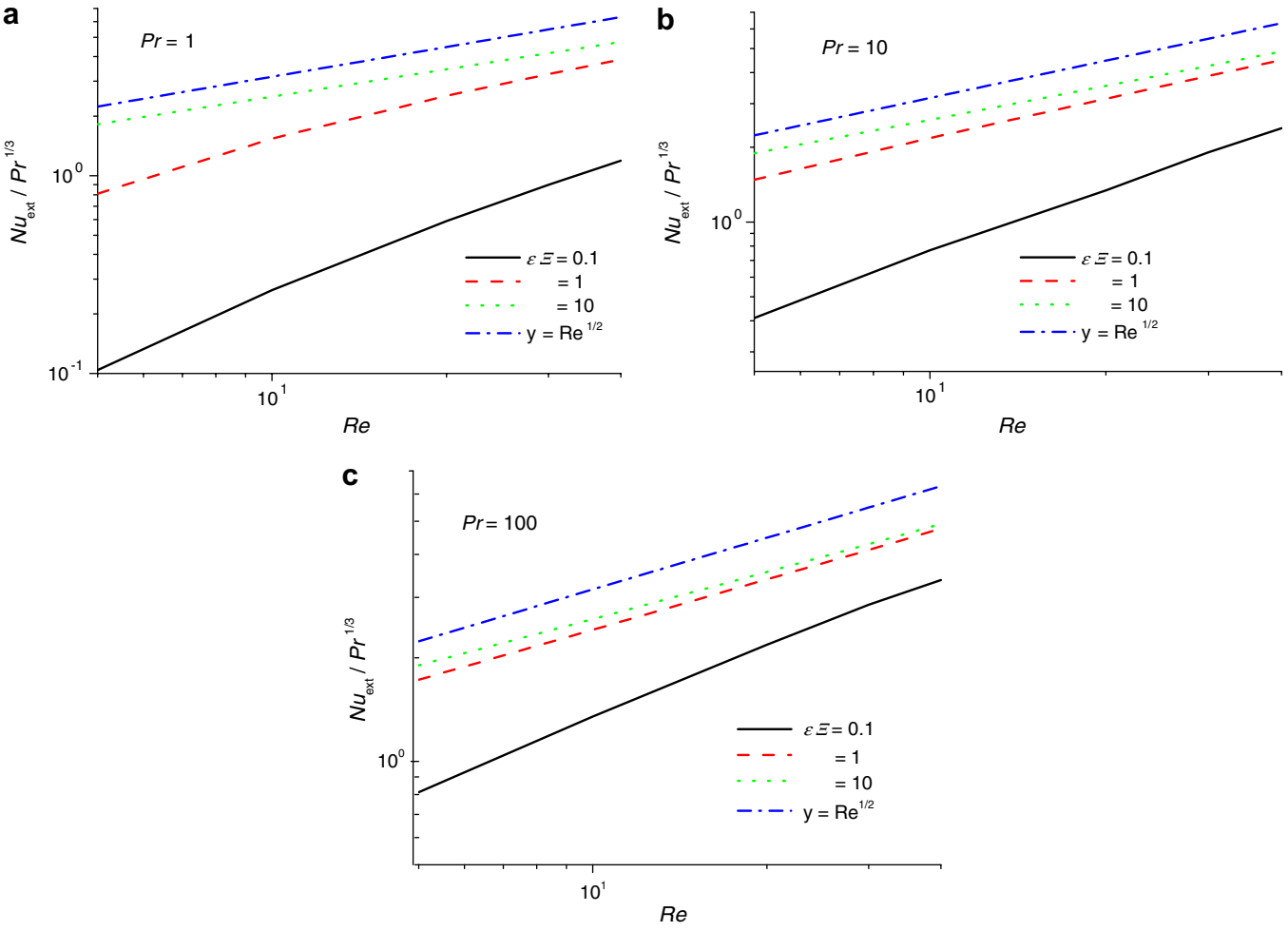

Fig. 4. Variation of the heat transfer group $Nu_{ext}/Pr^{1/3}$ with Re number for $\varepsilon = 0.1$; (a) $Pr = 1$; (b) $Pr = 10$; (c) $Pr = 100$.

Table 4
Heat transfer parameter values

Re	(Asymptotic Nu_{ext})/($Re^{1/2}Pr^{1/3}$)				
	$\varepsilon\Xi = 0.1$, $Pr = 1$		$\varepsilon\Xi = 10$, $Pr = 100$		
	$\varepsilon = 0.1$	$\varepsilon = 0.4$	$\varepsilon = 0.1$	$\varepsilon = 0.4$	$\varepsilon = 0.75$
5	0.0465	0.0339	0.850	0.793	0.6895
10	0.0835	0.0586	0.820	0.765	0.663
20	0.132	0.090	0.796	0.739	0.634
30	0.164	0.111	0.783	0.725	0.627
40	0.188	0.125	0.775	0.715	0.629

– for given *Re*, *Pr* and ε values, the heat transfer rate is strongly influenced by Ξ; the increase in Ξ increases the average *Nu* number values; when $\Xi \to \infty$, Nu_{ext} tends to the solutions provided by the elliptic cylinder with constant temperature; this behaviour is similar to that of the finite plate [16], cylinder [17] and sphere [18,19];
– for large values of $\varepsilon\Xi$ and small values of the aspect ratio, the asymptotic values of the elliptic cylinder *Nu* number are approximately equal to those of the flat plate; for small $\varepsilon\Xi$ values, the difference between the elliptic cylinder and finite plate results increases; the thermal wake phenomenon [16,20] is the explanation of this situation; the increase in the curvature of the surface of transfer increases thermal wake;
– for given *Re*(*Pr*), $\varepsilon\Xi$ and ε values, the increase in *Pr*(*Re*) increases Nu_{ext}.

We considered that it is not necessary to present distinct plots for the dimensionless temperature of the cylinders. The graphs are similar to those presented for the sphere, circular cylinder and finite plate. The influence of ε and Ξ on the time variation of dimensionless temperature of the elliptic cylinder may be related to that observed at average *Nu* numbers. The relations (2b) and (5b) express the connection between the dimensionless cylinder temperature and Nu_{ext}.

The heat transfer group (asymptotic Nu_{ext})/$Pr^{1/3}$ is plotted vs. the *Re* number in Fig. 4 ($\varepsilon = 0.1$), 5 ($\varepsilon = 0.4$) and 6 ($\varepsilon = 0.75$). We selected these three values for the following reasons: for $\varepsilon = 0.1$ the elliptic cylinder approaches the flat

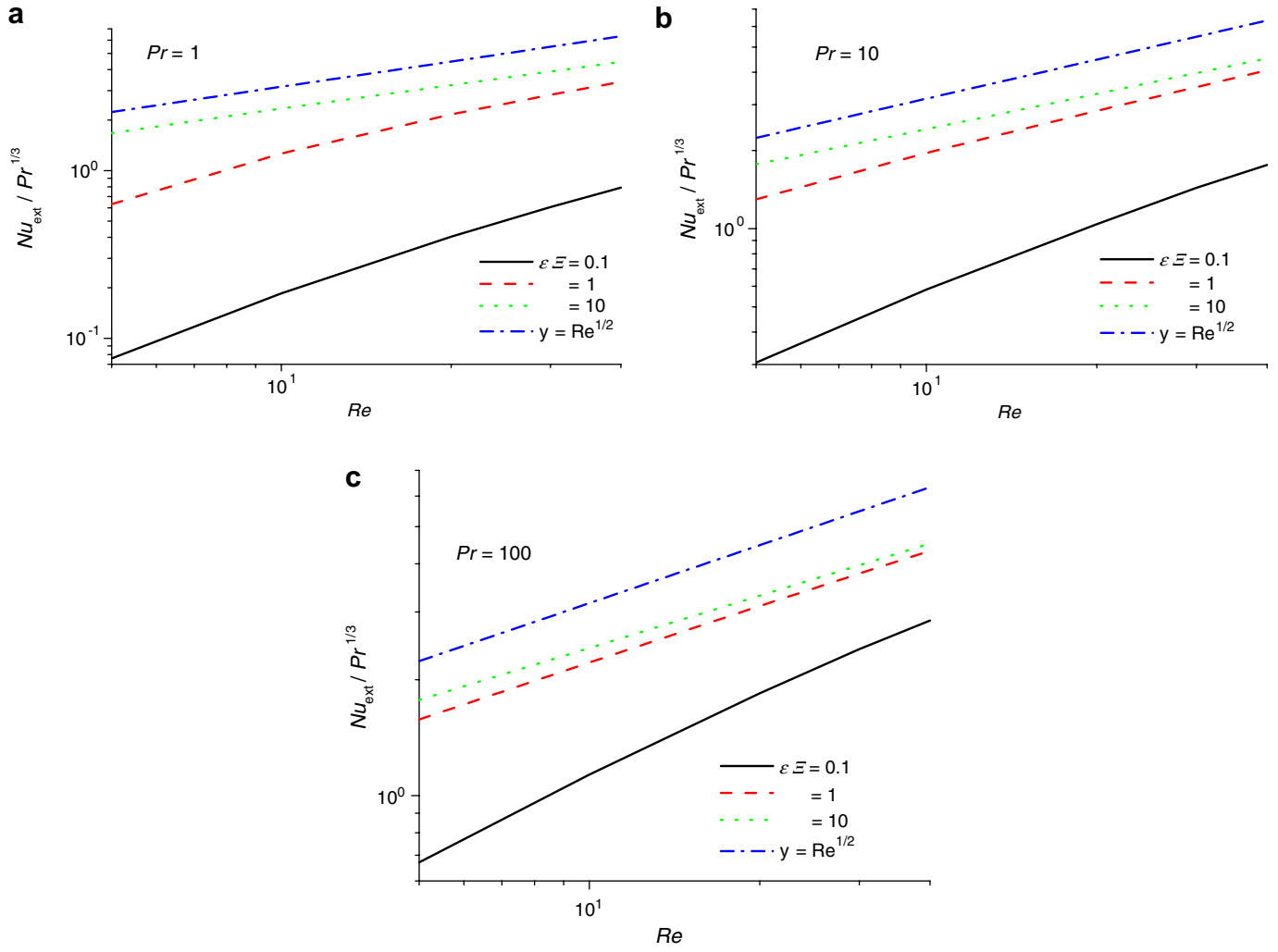

Fig. 5. Variation of the heat transfer group $Nu_{ext}/Pr^{1/3}$ with *Re* number for $\varepsilon = 0.4$; (a) $Pr = 1$; (b) $Pr = 10$; (c) $Pr = 100$.

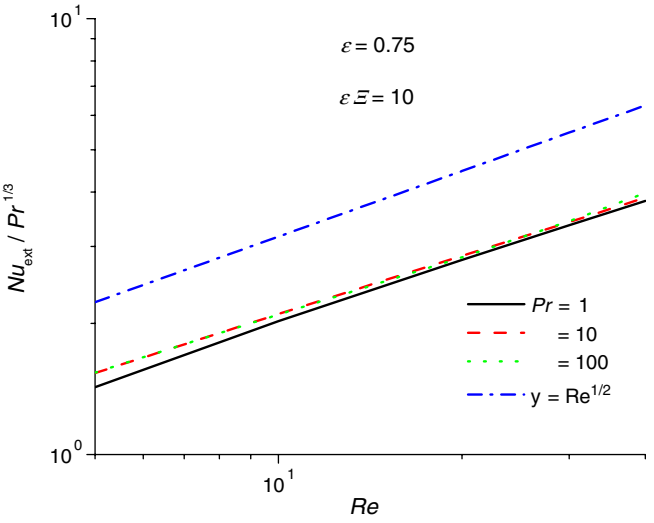

Fig. 6. Variation of the heat transfer group $Nu_{ext}/Pr^{1/3}$ with Re number for $\varepsilon = 0.75$ and $\varepsilon\Xi = 10$.

plate; for $\varepsilon = 0.75$ the elliptic cylinder approaches the circular cylinder; the case $\varepsilon = 0.4$ may be considered the intermediate case. For $\varepsilon = 0.75$ only the results obtained for $\varepsilon\Xi = 10$ may be considered relevant for the present analysis. For $\varepsilon = 0.75$ and $\varepsilon\Xi = 0.1$ and 1, the time variation of Nu_{ext} does not stabilize. In some cases oscillations occur. Table 4 presents the values of the heat transfer parameter (asymptotic Nu_{ext})/($Re^{1/2}Pr^{1/3}$) calculated for $Pr = 1$, $\varepsilon\Xi = 0.1$, $\varepsilon = 0.1$, 0.4 and $Pr = 100$, $\varepsilon\Xi = 10$, $\varepsilon = 0.1$, 0.4, 0.75.

Figs. 4–6 and Table 4 show that:

- for each of the cases presented in Figs. 4–6 the slope of the curves is different from 1:2; each curve has a different slope depending on Pr, $\varepsilon\Xi$ and ε; only for $\varepsilon\Xi = 10$ the influence of Pr may be considered negligible;
- for $Pr = 1$, $\varepsilon = 0.1$, 0.4, $\varepsilon\Xi = 0.1$, 1, $Pr = 1$, $\varepsilon = 0.75$, $\varepsilon\Xi = 10$ and $Pr = 10$, $\varepsilon = 0.4$, $\varepsilon\Xi = 0.1$, the curves are not straight lines; they exhibit a small curvature;
- the heat transfer parameter $Nu_{ext}/(Re^{1/2}Pr^{1/3})$ depends on Re, ε and $\varepsilon\Xi$; for $Pr = 100$ and $\varepsilon\Xi = 10$, $Nu_{ext}/(Re^{1/2}Pr^{1/3})$ converges to a value independent on Re.

The previous results show that a general correlation similar to that derived in [6] is not possible for the present situation. Practically, for each set (Pr, ε, $\varepsilon\Xi$) an independent relation should be worked out. Also, for some parameter values, any type of correlations cannot be established due to the time variation of the Nu number. For these reasons, we consider that for $Re \leqslant 40$, the solution to the unsteady heat transfer from an elliptic cylinder with spatially uniform, but changing with time temperature, is the numerical simulation.

References

[1] H.M. Badr, Mixed convection from a straight isothermal tube of elliptic cross-section, Int. J. Heat Mass Transfer 37 (1994) 2343–2365.
[2] S.J.D. D'Alessio, S.C.R. Dennis, Steady laminar forced convection from an elliptic cylinder, J. Eng. Math. 29 (1995) 181–193.
[3] S.J.D. D'Alessio, Steady and unsteady forced convection past an inclined elliptic cylinder, Acta Mech. 123 (1997) 99–115.
[4] H.M. Badr, Forced convection from a straight elliptical tube, Heat Mass Transfer 34 (1998) 229–236.
[5] S.J.D. D'Alessio, M.G. Saunders, D.L. Harmsworth, Forced and mixed convective heat transfer from accelerated flow past an elliptic cylinder, Int. J. Heat Mass Transfer 46 (2003) 2927–2946.
[6] W.A. Khan, J.R. Culham, M.M. Yovanovich, Fluid flow around and heat transfer from elliptical cylinders: analytical approach, AIAA J. Thermophys. Heat Transfer 19 (2005) 178–185.
[7] E.W. Weisstein, Elliptic Cylindrical Coordinates. MathWorld. http://mathworld.wolfram.com/EllipticCylindricalCoordinates.html.
[8] Gh. Juncu, R. Mihail, Numerical solution of the steady incompressible Navier–Stokes equations for the flow past a sphere by a multigrid defect correction technique, Int. J. Num. Meth. Fluids 11 (1990) 379–395.
[9] Gh. Juncu, A numerical study of steady viscous flow past a fluid sphere, Int. J. Heat Fluid Flow 20 (1999) 414–421.
[10] B. Fornberg, A numerical study of steady viscous flow past a circular cylinder, J. Fluid Mech. 98 (1980) 819–855.
[11] P.W. Hemker, A numerical study of stiff two-point boundary problems. Ph. D. Thesis, Amsterdam, Mathematisch Centrum, 1977.
[12] P. Sivakumar, Ram Prakash Bharti, R.P. Chhabra, Steady flow of power-law fluids across an unconfined elliptical cylinder, Chem. Eng. Sci. 62 (2007) 1682–1702.
[13] S.J.D. D'Alessio, S.C.R. Dennis, A vorticity model for viscous flow past a cylinder, Comput. Fluids 23 (1994) 279–293.
[14] S.J.D. D'Alessio, Steady, unsteady and linear stability of flow past an elliptic cylinder, Can. Appl. Math. Quat. 4 (1996) 341–379.
[15] S.C.R. Dennis, P.J.S. Young, Steady flow past an elliptic cylinder inclined to the stream, J. Eng. Math. 47 (2003) 101–120.
[16] Gh. Juncu, Unsteady forced convection heat/mass transfer from a flat plate, Heat Mass Transfer 41 (2005) 1095–1102.
[17] Gh. Juncu, Unsteady conjugate heat/mass transfer from a circular cylinder in laminar crossflow at low Reynolds numbers, Int. J. Heat Mass Transfer 47 (2004) 2469–2480.
[18] B. Abramzon, C. Elata, Unsteady heat transfer from a single sphere in Stokes flow, Int. J. Heat Mass Transfer 27 (1984) 687–695.
[19] Gh. Juncu, Unsteady heat and/or mass transfer from a fluid sphere in creeping flow, Int. J. Heat Mass Transfer 44 (2001) 2239–2246.
[20] Gh. Juncu, The influence of the continuous phase Pe numbers on thermal wake phenomenon, Heat Mass Transfer 34 (1998) 203–208.